# Seismic Collapse Response of Steel Moment Frames with Deep Columns

Tung-Yu Wu, S.M.ASCE<sup>1</sup>; Sherif El-Tawil, Ph.D., P.E., F.ASCE<sup>2</sup>; and Jason McCormick, Ph.D., P.E., A.M.ASCE<sup>3</sup>

Abstract: The seismic collapse behavior of 4-story and 8-story steel special moment frames (SMFs) with deep columns is investigated using computational simulation. The models used are capable of modeling local and global instabilities and explicitly representing both sidesway and vertical collapse behaviors. Three key factors that affect the collapse potential of the frames are studied: (1) column lateral bracing; (2) level of column gravity load; and (3) column section properties. It is shown that, even when they satisfy current seismic provisions, deep columns can suffer early global instability, leading to vertical system collapse at relatively low drift levels. The findings indicate that the performance of moment frames can be improved by limiting the axial load levels on exterior columns, carefully selecting member sizes to limit depth-thickness and overall slenderness of the columns, and providing adequate lateral bracing. It is suggested that column shortening, in itself, is a benign effect that does not compromise serviceability or contribute to the collapse of a well-designed frame. DOI: 10.1061/(ASCE)ST.1943-541X.0002150. © 2018 American Society of Civil Engineers.

#### Introduction

Deep steel columns (with a depth of 600 mm or greater) have been widely used in special moment frames (SMFs) since the late 1990s because of their suitability for satisfying post-Northridge seismic requirements. Although their vulnerability to torsional demands resulting from the formation of adjacent beam plastic hinges initially raised the concerns of researchers, the concerns were shown to be generally unfounded (Zhang and Ricles 2006; Chi and Uang 2002; Shen et al. 2002). Nevertheless, column behavior in these early studies was not fully addressed because the columns were not axially loaded.

A number of researchers noticed this issue and investigated the behavior of deep columns under combined drift and axial loading. Fogarty and El-Tawil (2015), Elkady and Lignos (2015a), and Ozkula et al. (2017) expressed concerns that current limits for local slenderness ratios ( $b_f/2t_f$  and  $h/t_w$ , where  $b_f$  is flange width, h is web height, and  $t_f$  and  $t_w$  are the flange and web thickness, respectively) cannot guarantee highly ductile behavior for deep columns, especially when the axial load is larger than  $0.2P_y$ , where  $P_y$  is the axial yield strength of the column cross section. The latest seismic design provisions (AISC 2016b) define highly ductile behavior as the ability to "withstand significant plastic rotation of 0.04 rad or more during the design earthquake."

Note. This manuscript was submitted on October 31, 2017; approved on March 26, 2018; published online on June 25, 2018. Discussion period open until November 25, 2018; separate discussions must be submitted for individual papers. This paper is part of the *Journal of Structural Engineering*, © ASCE, ISSN 0733-9445.

Initial concerns about deep columns may have been exacerbated by some of the assumptions used in the original studies. For example, Elkady and Lignos (2017), Fogarty et al. (2017), and Wu et al. (2018) noted that symmetric drift loading, which is commonly used in experimental research involving moment connections and used in early deep column studies, can be unrealistically severe. Based on an investigation of individual column behavior, Wu et al. (2018) proposed modified web limiting ratios that consider the effect of axial loads and global slenderness ratios ( $L/r_y$ , where L is the unbraced column length and  $r_y$  is the radius of gyration about the column's weak-axis) to ensure highly ductile behavior of such members under meaningful drift protocols.

Only a handful of studies investigated the effects of deep column behavior on the overall response of SMF systems. Reyes-Salazar et al. (2014) and Elkady and Lignos (2014, 2015b) conducted system-level studies of SMFs with deep columns. However, they used beam-column elements to model column response. The elements used could not capture the full range of instabilities that occur in deep columns, especially the formation of local buckling and interactions between local and global buckling. Using detailed finite-element models, Wu et al. (2017) explicitly considered the effect of local and global instabilities in deep columns on SMF behavior, but only with a limited set of variables.

The preceding survey shows that there is insufficient information about how SMFs with deep columns behave under severe seismic loading. To address this shortcoming, this study uses highfidelity models capable of capturing the local and global instabilities that occur in deep members under reversed cyclic loading and the complex interactions that occur between them. The study makes use of two prototype frames (four and eight stories) and focuses on the following key parameters that can influence frame collapse behavior under severe seismic loading: amount of lateral bracing; tributary gravity loads, and hence axial load level on columns; and column section properties. The collapse capacities of variants of the prototype frames are assessed using incremental dynamic analysis (IDA), as outlined by Vamvatsikos and Cornell (2002), and then used to evaluate the influence of each parameter on collapse response. The simulation results are used to critique current design guidelines and propose improved provisions.

<sup>&</sup>lt;sup>1</sup>Ph.D. Candidate, Dept. of Civil and Environmental Engineering, Univ. of Michigan, Ann Arbor, MI 48109-2125 (corresponding author). ORCID: https://orcid.org/0000-0002-2981-1910. Email: tungyuwu@umich.edu

<sup>&</sup>lt;sup>2</sup>Professor, Dept. of Civil and Environmental Engineering, Univ. of Michigan, Ann Arbor, MI 48109-2125. Email: eltawil@umich.edu

<sup>&</sup>lt;sup>3</sup>Associate Professor, Dept. of Civil and Environmental Engineering, Univ. of Michigan, Ann Arbor, MI 48109-2125. Email: jpmccorm@umich.edu

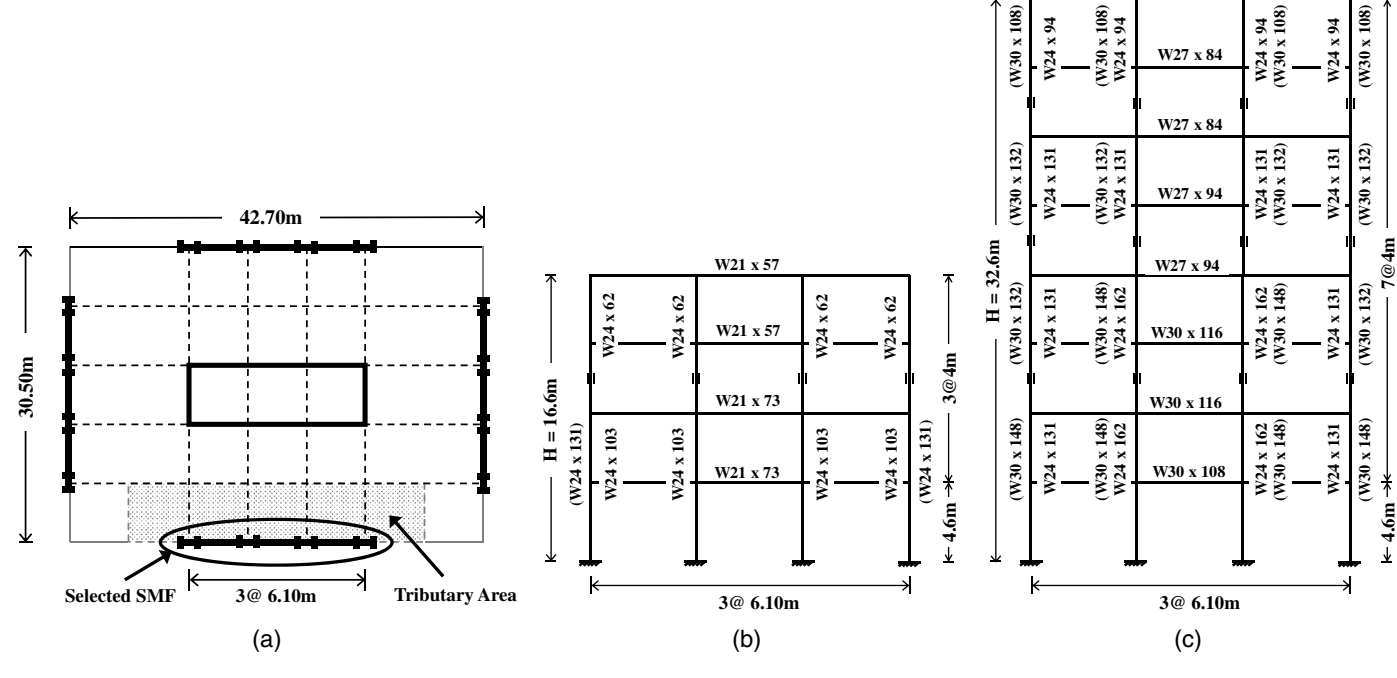


**Fig. 1.** (a) Typical plan configuration; (b) elevation view of 4-story prototype SMF; and (c) elevation view of 8-story prototype SMF. Column sections of variants S4-L1-T3-C2 and S8-L1-T2-C3 are shown in parentheses.

## **Prototype Frames**

This study used 4-story and 8-story SMFs as prototype frames. The frames were designed by NIST (2010) using response spectrum analysis (RSA) for seismic design category  $D_{\rm max}$ . The location of the selected frames is circled in the typical plan configuration shown in Fig. 1(a). The locations of tributary gravity loads allocated to the frames are shaded in Fig. 1(a). Perimeter SMFs are assumed to resist all the seismic loading on the building.

The frames were designed with W24 columns and reduced beam sections (RBS) using ASTM A992 steel per AISC (2005a, b) and ASCE (2005). As is customary, the beam and column sections used in the 4-story and 8-story frame are listed in English units

(in.  $\times$  lb/ft) in Figs. 1(b and c), respectively. The columns were spliced every two stories. Although the frames were designed in accordance with 2005 codes, the 4-story frame also satisfied the latest specifications, i.e., AISC (2016a, b) and ASCE (2016). On the other hand, the 8-story frame did not fulfill the strong columnweak beam requirement in AISC (2016b). This is because, unlike AISC (2005b), the required column axial compressive strength used in the calculation of the column-beam moment ratio in AISC (2016b) incorporates the overstrength seismic load, the inclusion of which significantly reduces the moment capacity of the columns. Table 1 lists key properties of the prototype 4-story and 8-story frames (labeled S4-L1-T2-C1 and S8-L1-T2-C2, respectively). The table lists the fundamental period ( $T_1$ ) along with slenderness

W21 x 68

Table 1. Properties and collapse analysis results of prototype frames and variants

	Lateral	Gravity	Column					$\tilde{S}_{a,C}(T_1,5\%)$	$\tilde{SDR}_{max,C}$			mber
Frame identifier	bracing	loads	section <sup>a</sup>	$h/t_w^a$	$L/r_y^a$	$P_g/P_y^{a}$	$T_1$ (s)	(g)	(%)	$\lambda_c$	SC	VC
4-story												
S4-L1-T1-C1	LBC1	TGL1	$W24 \times 103$	39.2	79.8	0.11	1.67	0.68	8.0	$4.18 \times 10^{-4}$	11	0
S4-L1-T2-C1	LBC1	TGL2	$W24 \times 103$	39.2	79.8	0.18	1.67	0.65	7.5	$4.43 \times 10^{-4}$	10	1
S4-L1-T3-C1	LBC1	TGL3	$W24 \times 103$	39.2	79.8	0.27	1.67	0.50	4.2	$7.02 \times 10^{-4}$	3	8
S4-L2-T1-C1	LBC2	TGL1	$W24 \times 103$	39.2	90.5	0.11	1.67	0.68	8.0	$4.20 \times 10^{-4}$	11	0
S4-L2-T2-C1	LBC2	TGL2	$W24 \times 103$	39.2	90.5	0.18	1.67	0.64	7.0	$4.63 \times 10^{-4}$	9	2
S4-L2-T3-C1	LBC2	TGL3	$W24 \times 103$	39.2	90.5	0.27	1.67	0.42	3.0	$9.99 \times 10^{-4}$	0	11
S4-L3-T1-C1	LBC3	TGL1	$W24 \times 103$	39.2	19.9	0.11	1.67	0.70	8.2	$3.87 \times 10^{-4}$	11	0
S4-L3-T2-C1	LBC3	TGL2	$W24 \times 103$	39.2	19.9	0.18	1.67	0.67	7.7	$4.12 \times 10^{-4}$	11	0
S4-L3-T3-C1	LBC3	TGL3	$W24 \times 103$	39.2	19.9	0.27	1.67	0.62	7.3	$4.83 \times 10^{-4}$	10	1
S4-L1-T3-C2	LBC1	TGL3	$W24 \times 131$	35.6	53.5	0.21	1.64	0.67	7.4	$4.09\times10^{-4}$	10	1
8-story												
S8-L1-T2-C2	LBC1	TGL2	$W24 \times 131$	35.6	50.6	0.27	2.37	0.54	7.7	$1.76 \times 10^{-4}$	11	0
S8-L1-T2-C3	LBC1	TGL2	$W30\times148$	41.6	65.9	0.24	2.21	0.60	5.4	$1.63 \times 10^{-4}$	3	8

Note: SC = sidesway collapse; and VC = vertical collapse.

<sup>&</sup>lt;sup>a</sup>Properties of first-story exterior columns.

properties of the first-story exterior columns. NIST (2010) provided further design details.

#### **Frame Variants**

Key parameters that influence member capacity and, in turn, system capacity, are (1) lateral bracing condition (LBC); (2) tributary gravity loads (TGLs); and (3) column section properties. A number of frame variants were created in order to investigate the effect of these parameters on system behavior.

## Lateral Bracing Condition

One of the primary parameters that determines a column's buckling strength is the unbraced length, L, which depends on the spacing of lateral bracing. In current seismic provisions (AISC 2016b), beam-column connections require lateral bracing at the levels of both the top and bottom beam flanges unless a column is shown to remain elastic outside of the panel zone. If the column remains elastic, which can be assumed when the column-beam moment ratio at the connections is larger than 2.0, the connection is permitted to be laterally braced only at the level of the top beam flanges. This typically happens for exterior columns, in which the beam moment resistance contribution comes from only one beam. The limit on the column-beam moment ratio is described as a "reasonable cutoff" (AISC 2016b) and its effect on overall system behavior is not yet well studied.

Three different lateral bracing conditions were considered for the 4-story frames: (1) beam-column connections were laterally braced at the levels of both the top and bottom beam flanges regardless of column-beam moment ratios at the connections (designated LBC1); (2) similar to the LBC1 condition, except that the lateral bracing of beam-column connections at the level of the bottom beam flanges was removed when the column-beam moment ratios at the connections were greater than 2.0 (designated LBC2); and (3) similar to the LBC1 condition, except that additional lateral bracing was applied at quarter points along the column height (designated LBC3).

Frames with LBC2 were compared with those with LBC1 to study the effect of removing lateral bracing at the bottom beam flanges allowing for evaluation of the "reasonable cutoff" comment in current provisions (AISC 2016b). LBC3 was meant to greatly reduce the possibility of out-of-plane flexural buckling and lateral torsional buckling of columns in order to understand the general influence of column instabilities on frame collapse capacity. It is acknowledged that LBC3 is an impractical condition to achieve, but it nevertheless provides important insight into the effects of bracing on system behavior. Fig. 2 shows the three LBC conditions.

## **Tributary Gravity Loads**

Wu et al. (2018), Fogarty et al. (2017), Fogarty and El-Tawil (2015), Ozkula et al. (2017), and Elkady and Lignos (2015a) showed that the initial column axial force, which results from gravity loading, plays an important role in determining the cyclic responses of deep columns. Therefore, this study also selected the axial load ratio of first-story exterior columns,  $P_g/P_y$ , induced by the tributary gravity loads as a key parameter;  $P_g$  is the gravity load and  $P_y$  is the yield capacity of the cross section of the column. The  $P_g/P_y$  ratio under the TGL in Fig. 1(a) using the load combination of 1.05D + 0.25L per FEMA P695 (FEMA 2009) is 0.18 for the 4-story frame. The level of axial load caused by this tributary area is designated TGL2. To explore the effect of TGL on the collapse capacity of the SMF, a lower level ( $P_g/P_y = 0.11$ , TGL1) and a

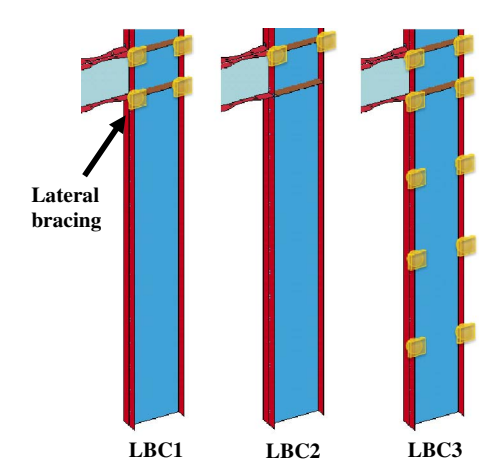


Fig. 2. Lateral bracing conditions.

higher level  $(P_g/P_y = 0.27, \text{TGL3})$  were used to reflect smaller and greater tributary areas, respectively. The TGL1 and TGL3 cases were considered to be reasonable and could correspond to feasible design situations. The seismic weight of the SMF in the three TGL cases remained unchanged to maintain the same seismic force.

To account for all possible combinations of LBC and TGL conditions, eight variants of the 4-story frame were created in addition to the prototype frame. A descriptive naming scheme was used in order to facilitate discussion of the key parameters. For example, the prototype 4-story frame was designated S4-L1-T2-C1, where S4, L1, and T2 stand for 4-story, LBC1, and TGL2, respectively, and C1 refers to W24  $\times$  103 sections as first-story exterior columns. Following the same designation, the variant S4-L3-T2-C1 was the 4-story frame with LBC3 and TGL2 conditions and W24  $\times$  103 exterior columns. Table 1 lists details of the variants.

## Column Section Properties

In addition to the initial axial load, the web slenderness ratio  $(h/t_w)$  and global slenderness ratio  $(L/r_y)$  have also been shown to be significant factors affecting deep column capacity (Fogarty and El-Tawil 2015; Wu et al. 2018). To study their potential influence on frame capacity, another variant was created by replacing the first-story exterior columns of the S4-L1-T3-C1 frame with a W24 × 131 section, which had a slightly smaller  $h/t_w$  and much smaller  $L/r_y$  than the original W24 × 103 section. The variant was designated S4-L1-T3-C2, where C2 refers to W24 × 131 section [Fig. 1(b)].

To further investigate the effect of  $L/r_v$ , the prototype 8-story frame (S8-L1-T2-C2 in Table 1) was redesigned using W30 shapes as column sections in accordance with the latest specifications (AISC 2016a, b; ASCE 2016). The redesigned frame, which had a larger exterior column  $L/r_v$  than the prototype, is shown in Fig. 1(c) with the column sections in parentheses. It is termed S8-L1-T2-C3 in Table 1, where C3 refers to the W30  $\times$  148 section. The larger  $L/r_v$  necessitated the use of a heavier section (W30 × 148) for first-story exterior columns in order to satisfy strength requirements. The W30 × 148 section was also used for interior columns. Even though it was lighter than that originally used (W24 × 162), it satisfied design requirements, including the more stringent strong column-weak beam requirement in AISC (2016b). As a result, the S8-L1-T2-C3 frame had a similar weight to S8-L1-T2-C2, but higher system flexural stiffness, i.e., shorter fundamental period  $T_1$ .

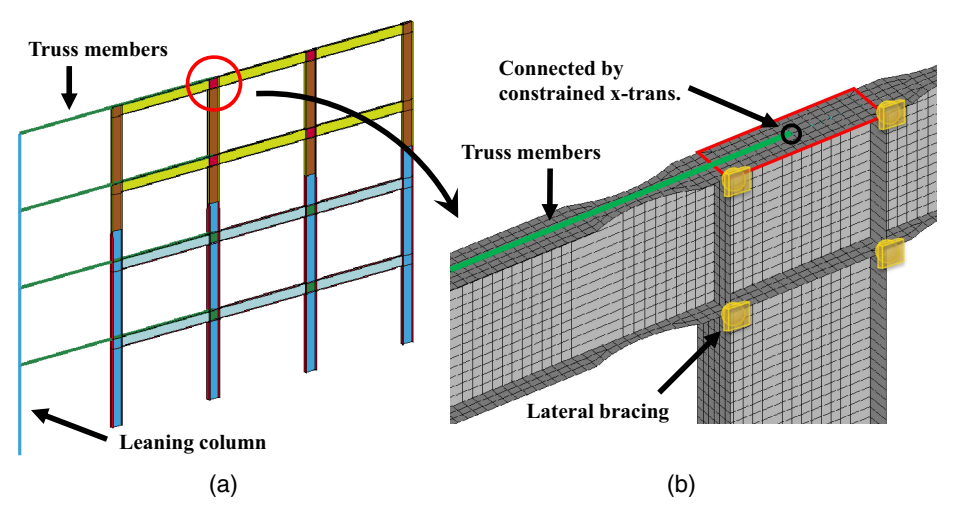


Fig. 3. Finite-element models of (a) 4-story SMFs; and (b) beam-to-column connections.

## **Finite-Element Modeling**

### Modeling Approach

Detailed finite-element models of the SMF were created in Hypermesh (2013) and analyzed using the explicit solver implemented in LS-DYNA (2013), a commercial platform. The building model was discretized using 3-node and 4-node fully integrated shell elements (ELFORM 16) based on the formulation published by Engelmann et al. (1989) (Fig. 3). A combined isotropic/kinematic hardening material model (MAT\_153) developed by Huang and Mahin (2010) was used to represent material behavior. The hardening moduli and model parameters were calibrated to the true stress—true strain model proposed by Arasaratnam et al. (2011). The model divided the constitutive relationships into five stages and was calibrated to capture the behavior of A992 steel well into the postultimate strength range. The calibration was the same as that used by Wu et al. (2018) (Fig. 4).

The SMF was assumed to be fully fixed at its base. The lateral bracing of the SMF was simulated by preventing out-of-plane translation at key nodes [Fig. 3(b)]. Both flanges of the beams were laterally braced at locations with a spacing  $L_b$  that satisfied the

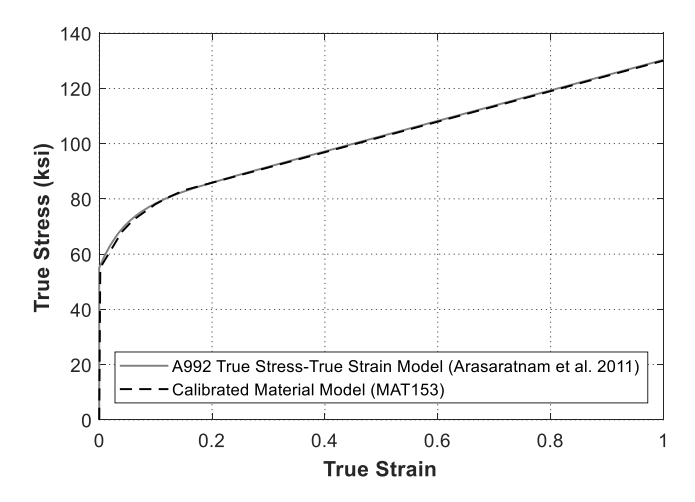


**Fig. 4.** Material model calibration with true stress-true strain model for A992 steel. (Reprinted from Wu et al. 2018, © ASCE.)

requirement for highly ductile members in AISC (2016b). Column flanges were laterally braced at locations based on the SMFs' LBC. Systemwide P-delta effects were considered by connecting a leaning column to the SMF with rigid truss members [Fig. 3(a)]. The rigid truss member at each floor was attached to the center point of the continuity plate for beam top flanges with an x-translation constraint [Fig. 3(b)]. A gravity load equal to half of the building floor mass minus that distributed to the SMF system according to its TGL was applied at each floor of the leaning column. Because the use of stiffness-proportional damping considerably reduces the time step in explicit schemes, only mass-proportional damping was considered (Xiaoming et al. 2015). A mass-proportional damping of 2.5% was assumed at the first mode period of each SMF. Imperfections were deliberately not included to avoid favoring predetermined instability modes.

The finite-element models of the 4-story and 8-story frames consisted of approximately 96,000 and 235,000 elements, respectively. The simulations ran on a cluster with 16 processors. The simulation time to model 30 s of real time was about 30 and 57 h for the 4-story and 8-story prototype frames, respectively. A total of 836 simulations were performed.

## Collapse Criteria

The collapse behavior of SMFs under seismic loading is commonly categorized into two mechanisms: sidesway collapse and vertical collapse. Sidesway collapse, which occurs when the lateral resistance of the SMF is overcome by P-delta effects due to excessive lateral displacements, has been extensively studied in previous research (Zareian et al. 2010; Eads et al. 2013; Hamidia et al. 2014). On the other hand, vertical collapse, which is initiated by the inability of columns to support gravity loads, has not received as much attention as it deserves, particularly in the presence of deep wide flange columns. To thoroughly investigate the influence of column behavior, this study considered both collapse modes.

Two types of sidesway mechanisms are observed: first-story and multistory mechanisms. Fig. 5 shows the progression of a first-story mechanism for S8-L1-T2-C2 subjected to the ground motion record Northr/MUL009. The collapse process began with extensive local buckling at the bottom ends of the first-story columns and the RBS regions in the beams at about 22 s. The local instabilities resulted in strength and stiffness deterioration of the columns and impaired the lateral resistance of the frame, accelerating the drift

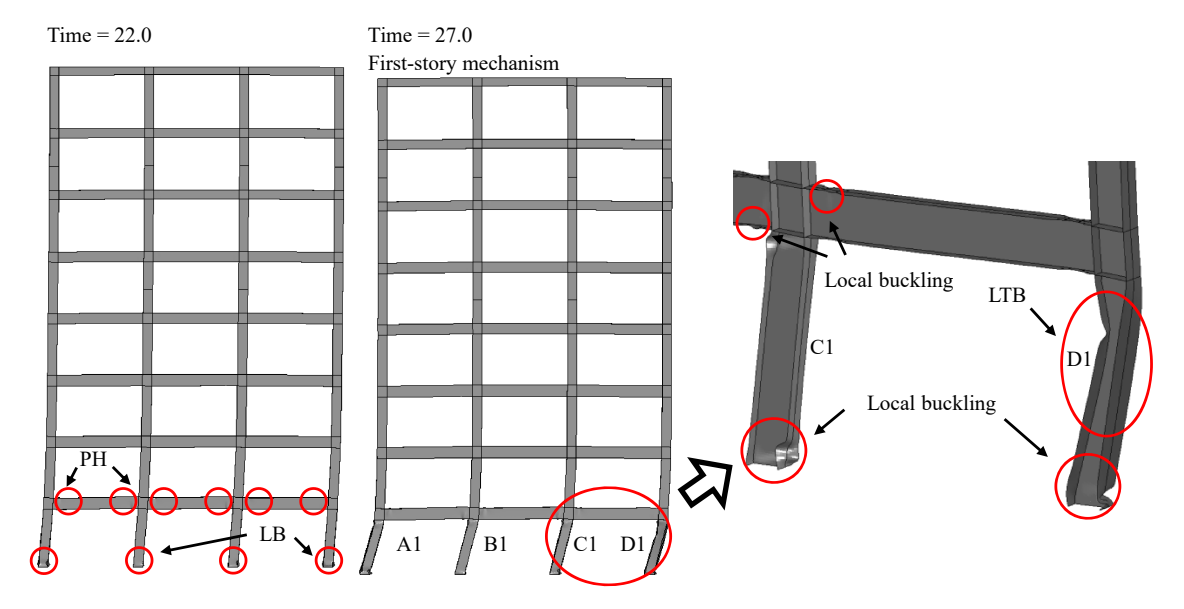


Fig. 5. Progression of first-story mechanism. PH = plastic hinges; LB = local buckling; and LTB = lateral torsional buckling.

response. At about 27 s, the P-delta effect became large enough to overcome lateral resistance, triggering the formation of a first-story mechanism.

Modeling the sidesway collapse process can be computationally expensive because in many cases the SMF continues to lean over slowly after the end of the imposed seismic loading until it reaches equilibrium and stops or continues to complete collapse. Therefore, to limit the computational effort, which is proportional to the simulated time in explicit integration schemes, as used herein, the maximum simulated time was determined as the time needed for the Arias intensity to reach 95% ( $t_{IA=95\%}$ , Arias 1970) plus 10 s. For example, the simulation was terminated at 27.64 s for the ground motion record Northr/MUL009, which has a  $t_{IA=95\%}$  of 17.64 s. Sidesway collapse was assumed to occur during this time frame if 1) the maximum story drift ratio (SDR) surpassed 10%, or 2) story drift ratio increased 2% or more during the last 10 s window of simulated time.

The former criterion is a reasonable lateral deformation limit attributed to Vamvatsikos and Cornell (2002) and commonly used

by others. The latter criterion is based on the observation that the closer the SMF is to collapse, the faster is its rate of drift. This trend is seen in Fig. 6(a), which shows the first-story drift ratio history of the S4-L1-T1-C1 frame subjected to the ground motion record Hector/HEC000 scaled to increasing  $S_a(T_1, 5\%)$ , the 5% damped spectral accelerations at the fundamental period. The two vertical dashed lines represent the 10 s interval after  $t_{IA=95\%}$ . As the spectral acceleration increased, the story drift history not only reached a larger drift level, but also increased at a faster rate. This phenomenon can be better appreciated in Fig. 6(b), which plots the relationship between  $S_a(T_1, 5\%)$  and  $v_{SDR}$ , the story drift ratio rate (%/sec) averaged over the last 10 s of simulated time. It is obvious that  $v_{\rm SDR}$ increased faster as  $S_a(T_1, 5\%)$  increased, signaling that the SMF was on its way to sidesway collapse as the seismic intensity increased. Based on numerous simulations that explored how frames undergo sidesway collapse, it was found that the 2% threshold signaled eventual sidesway collapse.

Unlike sidesway collapse, vertical collapse can be clearly identified from the deformed shape of the frame. Vertical collapse

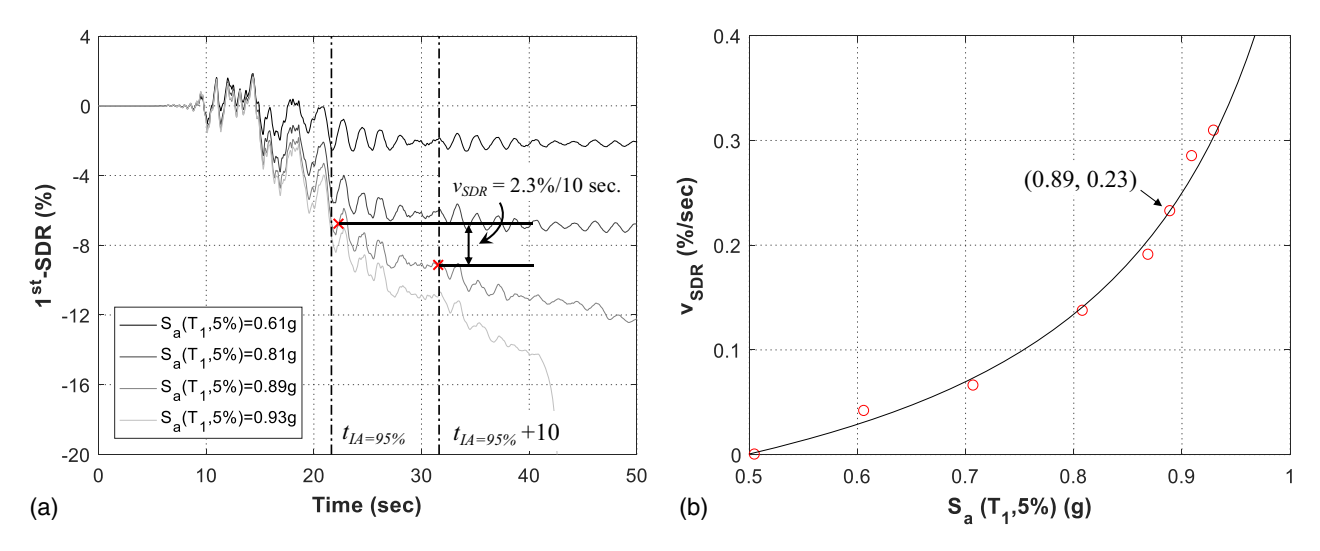


Fig. 6. (a) First-story drift ratio history; and (b) story drift ratio rate averaged over the 10 s ( $v_{\rm SDR}$ , %/s) of the S4-L1-T1-C1 frame subject to Hector/HEC000 record with different  $S_a(T_I, 5\%)$ .

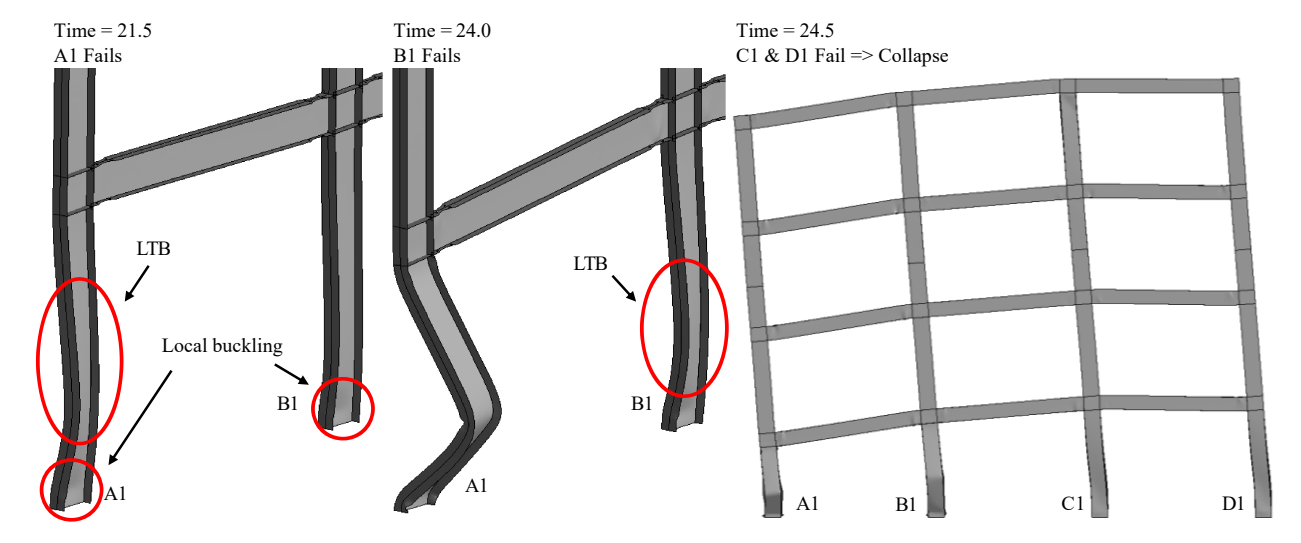


Fig. 7. Progression of vertical collapse for S4-L1-T3-C1 frame subject to Hector/HEC000 record with  $S_a(T_1, 5\%) = 0.71g$ .

usually begins with column failure, followed by a redistribution of gravity loads, leading to successive failures of adjacent columns and eventually a vertical progressive collapse scenario (Fig. 7). The axial force in exterior Column A1 fluctuated about its initial level (caused by gravity loads) due to the overturning moments caused by seismic shaking. As Column A1 failed due to flexural buckling and lost its ability to carry the imposed axial load demands (time  $= 21.5 \, \text{s}$ ), the adjacent Column B1 attempted to take over Column A1's share of the load, but was unable to (time  $= 24.0 \, \text{s}$ ). The successive loss of column axial capacity led to vertical progressive collapse of the SMF at time  $= 24.5 \, \text{s}$ .

#### Validation

The finite-element modeling approach used in this study was validated using experimental data provided by Ozkula et al. (2017) in their cyclic tests of deep columns. Twenty-five W24 beamcolumn specimens were tested under the symmetric cyclic lateral loading scheme combined with various levels of axial loads. The specimens were 5.49 m long, made of A992 steel, and fixed at both ends. The finite-element models of the specimens were created using the modeling approach described in the previous section, except that the material properties documented in Ozkula et al. (2017) were used in the true stress-true strain model. The validation results show that the cyclic responses of the specimens, including postyield stiffness, strength degradation rate, local buckling behavior, and failure modes, were reasonably captured by the finite-element models. Fogarty et al. (2017) provided more details about the validation studies. They are not repeated here in the interest of conserving space.

#### Simulation Results

The collapse capacities of the SMFs in Table 1 were evaluated through finite-element analysis to study the influence of key parameters. FEMA P-58 (FEMA 2012) suggests that 11 pairs of motion (i.e. 22 records) should be used to adequately capture variability in ground motion. However, the high computational cost associated with running the frame models makes complying with this recommendation prohibitive. As a compromise between computational expediency and accuracy, the evaluation used 11 ground motion

**Table 2.** Ground motion records used in collapse evaluation of SMFs

Number	Event	Station	Component
1	Northridge, 1994	Beverly Hills—Mulhol	9
2	Northridge, 1994	Canyon Country—WLC	0
3	Duzce, 1999	Bolu	0
4	Hector Mine, 1999	Hector	0
5	Imperial Valley, 1979	Delta	262
6	Imperial Valley, 1979	El Centro Array #11	140
7	Kobe, 1995	Nishi-Akashi	0
8	Kobe, 1995	Shin-Osaka	0
9	Kocaeli, 1999	Duzce	180
10	Kocaeli, 1999	Arcelik	0
11	Landers, 1992	Yermo Fire Station	270

records (one from each of 11 pairs) selected from the far-field record set in FEMA P695 (FEMA 2009) (Table 2).

Incremental dynamic analysis (Vamvatsikos and Cornell 2002) was applied to obtain the collapse parameters associated with each record, i.e. spectral acceleration,  $S_{a,C}(T_1,5\%)$ , and maximum story drift ratio at frame collapse, SDR<sub>max,C</sub>, when one of the collapse criteria is met under the scaled record. The obtained  $S_{a,C}(T_1,5\%)$  and SDR<sub>max,C</sub> were used to determine the collapse fragility curves of each SMF by fitting the data to a lognormal distribution using the collapse fragility tool in FEMA P-58 (FEMA 2012). The mean annual frequencies of collapse,  $\lambda_c$ , were also computed by numerically integrating the collapse fragility curves with the seismic hazard curves, as Ibarra and Krawinkler (2005) did. The frames were assumed to be located at Square Park in Seattle (47.600, -122.300) with Site Class D. Seismic hazard data were obtained from the USGS (2018) using the 2008 update of Conterminous US.

Table 1 summarizes the analysis results, including the collapse capacity of each frame, i.e., the fitted median values of  $S_{a,C}$  and  ${\rm SDR}_{{\rm max},C},\,\tilde{S}_{a,C}$  and  ${\rm SDR}_{{\rm max},C}$ ; the mean annual frequencies of collapse,  $\lambda_c$ ; and the number of records causing different collapse modes. Figs. 8 and 9 plot the collapse fragility curves of the 4-story and the 8-story SMFs, respectively. For the assumed frame location, both 8-story frames exhibited  $\lambda_c < 2.01 \times 10^{-4}$  (Table 1), which is the current limit imposed by ASCE (2016) to achieve a 1% probability of collapse in 50 years. However, all the 4-story frames exhibited  $\lambda_c > 2.01 \times 10^{-4}$ , indicating that their risk for collapse was greater than that expected by current specifications. One key reason that the 4-story frames exhibits higher  $\lambda_c$  values

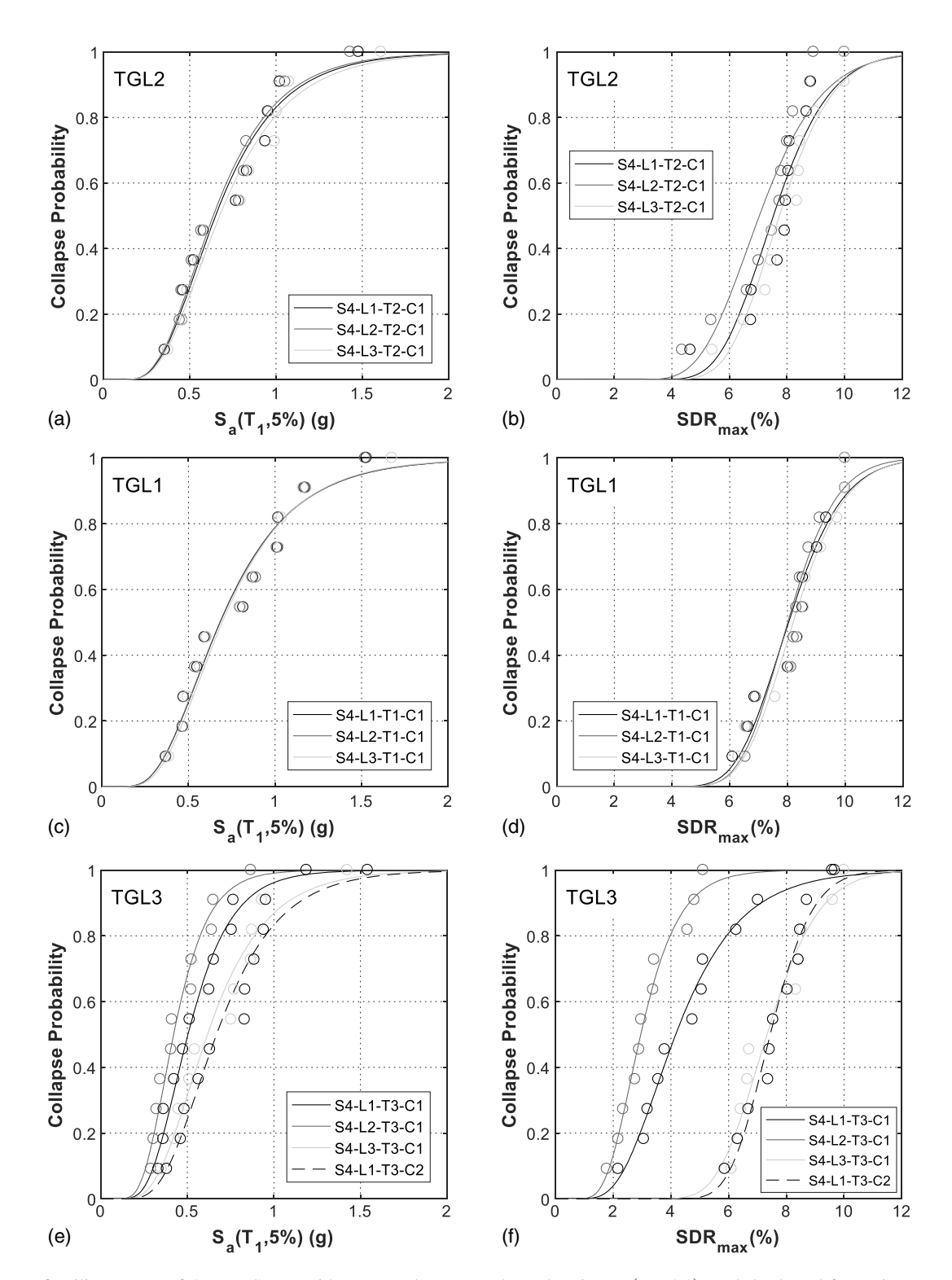


**Fig. 8.** Collapse fragility curves of 4-story SMFs with (a, c, and e) spectral acceleration  $S_a(T_1, 5\%)$ ; and (b, d, and f) maximum story drift ratio SDR<sub>max</sub> along x-axis.

than 8-story frames is the higher seismic hazard associated with the fundamental period of the 4-story frames versus the taller 8-story frames.

#### Effect of LBC and TGL

Table 1 and Fig. 8(a) show that lateral bracing had little effect on collapse response for the TGL2 condition. For example, the

collapse fragility curves in Fig. 8(a) were nearly identical to each other, and the median  $\tilde{S}_{a,C}$  and  $\lambda_c$  values in Table 1 were close to one another (0.65g and 4.43 × 10<sup>-4</sup> for S4-L1-T2-C1, 0.64g and 4.63 × 10<sup>-4</sup> for S4-L2-T2-C1, and 0.67g and 4.12 × 10<sup>-4</sup> for S4-L3-T2-C1). However, as shown in Fig. 8(b), there was a subtle difference: the collapse modes differed as listed in Table 1. For example, none of the seismic records caused vertical collapse of the S4-L3-T2-C1 frame, which had LBC3 conditions. On the other

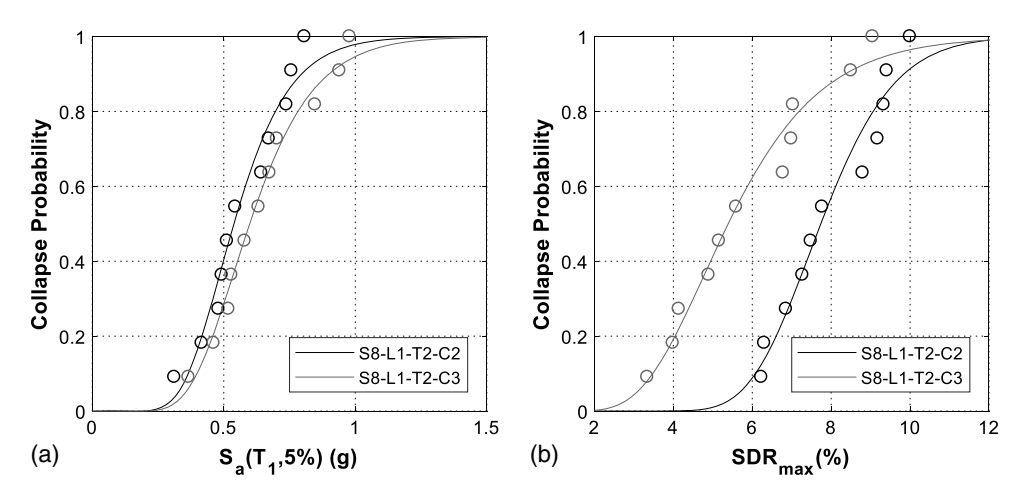


Fig. 9. Collapse fragility curves of 8-story SMFs with (a) spectral acceleration  $S_a(T_1, 5\%)$ ; and (b) maximum story drift ratio SDR<sub>max</sub> along x-axis.

hand, one and two records for the S4-L1-T2-C1 and S4-L2-T2-C1 frames, respectively, led to vertical collapse as the lateral bracing condition was eased.

Frames S4-L1-T2-C1, S4-L2-T2-C1, and S4-L3-T2-C1 also exhibited similar  $\tilde{SDR}_{max,C}$  values: 7.5% for S4-L1-T2-C1, 7.0% for S4-L2-T2-C1, and 7.7% for S4-L3-T2-C1 [Fig. 8(b)]. These levels of  $SDR_{max,C}$  were substantially higher than the achievable drift ratios seen in previous member level studies, e.g., Fogarty and El-Tawil (2015), Elkady and Lignos (2015a), and Ozkula et al. (2017). The discrepancy mainly resulted from that the fact that earlier studies used symmetric cyclic loading protocols, which impose more severe demands on the columns than actually occurs in the frame undergoing collapse. As explained by Wu et al. (2018) and observed by Elkady and Lignos (2017), the ratcheting behavior that occurs during collapse, which is obvious in Fig. 6(a) and was discussed by Krawinkler (2009), is substantially more benign than symmetric cyclic loading.

The effect of lateral bracing on collapse capacity was also small for frames with TGL1 conditions, i.e., the S4-L1-T1-C1, S4-L2-T1-C1, and S4-L3-T1-C1 frames. The  $\tilde{S}_{a,C}$ ,  $\tilde{SDR}_{max,C}$ , and  $\lambda_c$  values were almost identical for all three frames and for the collapse fragility curves, [Table 1 and Figs. 8(c and d)]. Unlike the TGL2 conditions, in which there were a few instances of vertical collapse, the three frames failed by sidesway collapse under all ground motion records.

At the other extreme, the TGL3 conditions, which imposed higher axial loads, greatly exacerbated instabilities in the columns, as evinced by the substantial sensitivity to the lateral bracing conditions [Figs. 8(e and f)]. For example, compared with the LBC1 conditions,  $\tilde{S}_{a,C}$  for the LBC2 conditions decreased from 0.50g to 0.42q (S4-L1-T3-C1 versus S4-L2-T3-C1) and increases to 0.62gfor the LBC3 case (S4-L1-T3-C1 versus S4-L3-T3-C1). The differences in  $\lambda_c$  also showed the significance of lateral bracing because the  $\lambda_c$  of S4-L2-T3-C1 is 42% higher than that of S4-L1-T3-C1 and double that of S4-L3-T3-C1. The effect was even more pronounced for SDR<sub>max,C</sub>. For example, SDR<sub>max,C</sub> of S4-L1-T3-C1, S4-L2-T3-C1, and S4-L3-T3-C1 was 4.2, 3.0, and 7.3%, respectively. The fact that  $\tilde{SDR}_{max,C}$  < 4.0% for S4-L2-T3-C1 and was just above 4.0% for S4-L1-T3-C1 is concerning because current specifications usually assume that a 4% drift level is achievable under design-level seismic loading. The comparatively poor performance under TGL3 conditions was caused by the vulnerability of deep columns to instability at higher axial loads, which compromises their ability to support axial load, promoting overall system failure.

The mode of failure for S4-L1-T3-C1 and S4-L2-T3-C1 changed from being primarily dominated by sidesway collapse under TGL1 conditions to mostly vertical collapse under TGL3 conditions (Table 1). The effect of axial load was substantial enough that one of the S4-L3-T3-C1 cases underwent vertical collapse in spite of the extensive lateral bracing provided by LBC3 conditions. Under seismic record Duzce/BOL000, the S4-L3-T3-C1 frame collapsed in a vertical progressive manner because the columns suffered extensive local buckling (Fig. 10).

Another key point is that the effect of TGL increased as TGL increased. For example,  $\tilde{S}_{a,C}$  for S4-L2-T1-C1 (TGL1,  $P_g/P_y=0.11$ ) was 0.68g. This decreased slightly to 0.64g for S4-L2-T2-C1 (TGL2,  $P_g/P_y=0.18$ ) and significantly to 0.42g for S4-L2-T3-C1 (TGL3,  $P_g/P_y=0.27$ ). The sharp increase of  $\lambda_c$  from 4.63 × 10<sup>-4</sup> for S4-L2-T2-C1 to 9.99 × 10<sup>-4</sup> for S4-L2-T3-C1 also reflected the trend. This effect is further emphasized in Fig. 11, which plots the relationship between  $P_g/P_y$  and SDR<sub>max</sub> for LBC1 conditions for various probabilities of collapse. Fig. 11 clearly shows the negative relationship between  $P_g/P_y$  and SDR<sub>max</sub> and that SRD<sub>max</sub> decreased rapidly when  $P_g/P_y$  surpassed about 0.2. For example, the probability of collapse before 4% drift was 10% and 20% for  $P_g/P_y=0.24$  and 0.25, respectively. In other words, a 1% increase in the gravity load:yield strength ratio caused a disproportionate 10% increase in the probability of collapse.

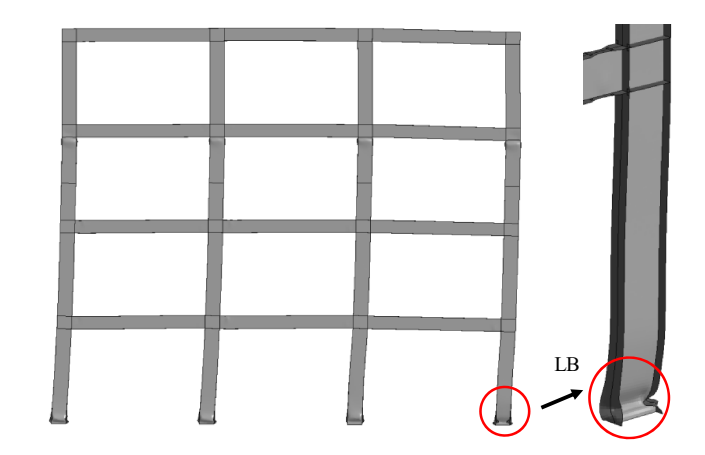


**Fig. 10.** Vertical collapse induced by severe local buckling in S4-L3-T3-C1 frame subject to Duzce/BOL000 record with  $S_a(T_1, 5\%) = 0.87g$ .

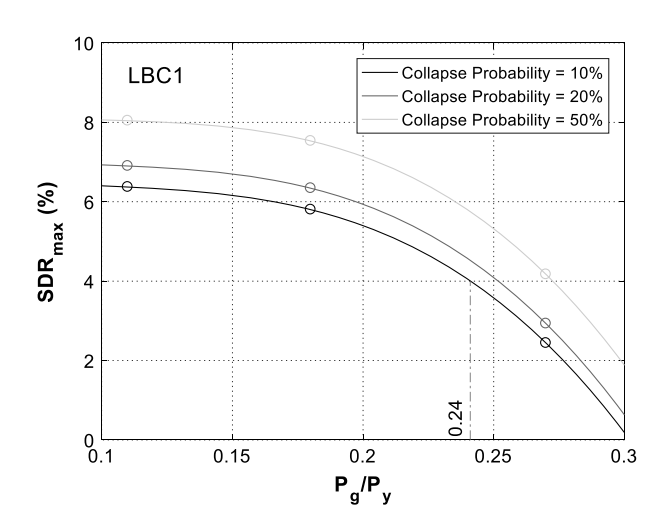


**Fig. 11.** Correlation trend between level of gravity loads and  $SDR_{max}$  with different collapse probabilities for 4-story frame with LBC1 conditions.

This high sensitivity to axial load level shows that an appropriate axial load limit should be specified in design specifications. The current AISC seismic provisions (AISC 2016b) do not include a limit, but CSA S-16 (CSA 2014) suggests a limit of  $0.3P_y$ . However, based on the presented research results,  $0.3P_y$  appears to be unconservative.

#### Effect of Column Section Properties

The first-story exterior columns of S4-L1-T3-C2 (W24 × 131) had a smaller  $h/t_w$  and significantly smaller  $L/r_y$  than those of S4-L1-T3-C1 (W24 × 103). Because these two frames were similar otherwise, as evinced by almost equal  $T_1$ , it is fair to compare their  $S_{a,C}$  values directly. Figs. 8(e and f) show the collapse fragility curves of frames with TGL3 conditions. S4-L1-T3-C2 was substantially better than S4-L1-T3-C1. For example,  $\tilde{S}_{a,C}$  increased from 0.50g for S4-L1-T3-C1 to 0.67g for S4-L1-T3-C2 and SDR<sub>max,C</sub> increased from 4.2 to 7.4%. Moreover, the dominant collapse mode changed from vertical collapse for S4-L1-T3-C1 to sidesway collapse for S4-L1-T3-C2 (Table 1). These results highlight the detrimental influence that a high  $L/r_y$  can have on overall system behavior.

Although frames S8-L1-T2-C2 and S8-L1-T2-C3 cannot be compared directly using their  $S_{a,C}$  and collapse fragility curves in Fig. 9(a) because of their different fundamental periods, their  $\lambda_c$  values show that the two frames had comparable risks of collapse  $(1.76\times10^{-4}~{\rm versus}~1.63\times10^{-4})$  in terms of spectral accelerations. However, S8-L1-T2-C2 had a much better drift capacity and therefore a higher SDR<sub>max,C</sub> (7.7%) compared with S8-L1-T2-C3 (SDR<sub>max,C</sub> = 5.4%) [Fig. 9(b) and Table 1]. Of particular concern is that one of the earthquake records caused collapse of S8-L1-T2-C3 at 3.3% drift. Moreover, S8-L1-T2-C2 consistently collapsed in sidesway mode, whereas S8-L1-T2-C3 collapsed in vertical collapse under 8 of the 11 ground motion records used (Table 1). These results suggest that S8-L1-T2-C2 has superior ductility to S8-L1-T2-C3 and a preferred failure mode.

The preceding results indicate that a SMF designed according to the latest specifications does not necessarily have better seismic performance than a SMF designed according to earlier AISC specifications in 2005. Even though the first-story exterior column of S8-L1-T2-C3 (W30  $\times$  148) had a slightly lower  $P_{\rm g}/P_{\rm y}$  than that

**Table 3.**  $P_{\text{max}}$  for first-story exterior columns

Frame	Column								
identifier	section	$P_g/P_y$	$P_{cl}/P_y$	$(P_g + P_{cl})/P_y$	$P_{\rm max}/P_{\rm y}$				
4-story									
S4-L1-T1-C1	$W24 \times 103$	0.11	0.15	0.26	0.27				
S4-L1-T2-C1	$W24 \times 103$	0.18	0.15	0.33	0.35				
S4-L1-T3-C1	$W24 \times 103$	0.27	0.15	0.42	0.43				
S4-L1-T3-C2	$W24 \times 131$	0.21	0.12	0.33	0.35				
8-story									
S8-L1-T2-C2	$W24 \times 131$	0.27	0.48	0.75	0.64				
S8-L1-T2-C3	$W30 \times 148$	0.24	0.44	0.68	0.59				

of S8-L1-T2-C2 (W24 × 131), the W30 × 148 section had higher web and global slenderness ratios,  $h/t_w$  and  $L/r_y$ , which offset the benefits of the lower axial demand. Fogarty et al. (2017) and Wu et al. (2018) identified these specific slenderness parameters as important factors for column capacity and they are the primary reason that S8-L1-T2-C3 performed worse than S8-L1-T2-C2 in spite of the heavier column section.

#### Axial Demands

Vertical collapse of SMFs is undesirable and results from global instability of column members. Table 3 lists  $P_{\rm max}$  for frames with LBC1 conditions, where  $P_{\rm max}$  is the maximum axial force in the first-story exterior columns during each earthquake, averaged across all records. Table 3 also shows the axial force that results from the capacity-limited seismic load effect,  $P_{cl}$ , as defined in AISC (2016b)

$$P_{cl} = \sum 2M_{pr,n} L_{h,n} \tag{1}$$

where  $L_{h,n}$  = distance between plastic hinge locations at the *n*th story; and  $M_{pr,n}$  = maximum probable moment at the location of the plastic hinge at the *n*th story as defined in AISC (2016a).

The sum of axial forces induced by gravity loads and capacity-limited effects, i.e.,  $P_g$  and  $P_{cl}$ , was generally slightly smaller than  $P_{\rm max}$  for the 4-story frame (Table 3). Eq. (1) underestimates  $P_{\rm max}$  because the strain hardening that takes place is underestimated in the computation of  $P_{cl}$ . For example, although AISC (2016a) assumes that strain hardening is 1.15 in the computation of  $M_{pr,n}$  of RBS connections made of A992 steel, values of about 1.25 were routinely seen in the 4-story frame used in this research. An opposite trend occurred in the 8-story frames, for which Eq. (1) substantially overestimated the capacity-limited effect (17 to 19%). This was directly attributed to higher vibration modes, as evidenced by the deformed shape of the vibrating frames, and suggests that even higher conservatism may be present for taller structures.

#### Column Axial Shortening

Several studies discussed the shortening behavior of deep columns subjected to combined axial and cyclic lateral loading (Elkady and Lignos 2015a; Ozkula et al. 2017; Elkady and Lignos 2017). Fogarty et al. (2017) showed that axial shortening is mainly attributed to flange and web local buckling and suggested that it can be controlled through compactness criteria. Elkady and Lignos (2017) noted that axial shortening is milder in a fixed-flexible column under collapse-consistent loading than in a fixed-fixed column under symmetric cyclic loading. Based on the small values they observed, Wu et al. (2018) considered axial shortening to be a serviceability issue. A common thread in all the preceding studies, which appear to have conflicting attitudes toward the importance

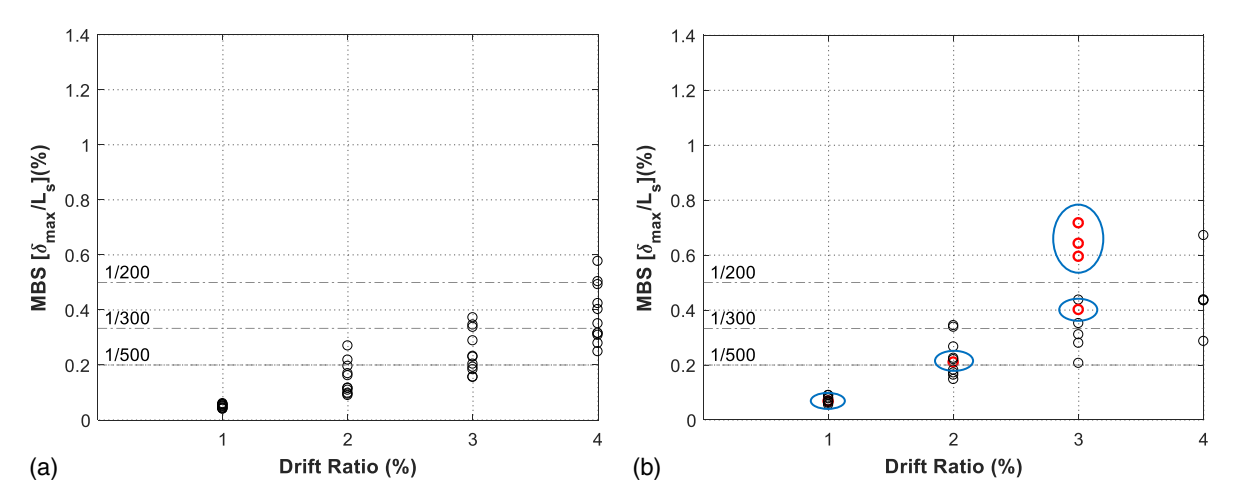


**Fig. 12.** Maximum beam slope evolution of beams framing into first-story columns in frames with LBC1 conditions under collapse-induced records: (a) S4-L1-T2-C1; and (b) S4-L1-T3-C1.

of the axial shortening phenomenon, is that the results were derived from component studies.

This study presented a unique opportunity to investigate this complex issue at the system level. To assess the extent of column shortening behavior during strong earthquake events, Fig. 12 plots the maximum beam slope (MBS) versus drift level. The MBS is the maximum of the vertical displacements ( $\delta_{\rm max}$ ) at the top of the four first-story columns normalized by beam span length ( $L_s$ ). Because the beams in the along-frame and transverse directions are equal in length ( $L_s=6.10$  m), MBS is essentially the maximum slope of the beams framing into the first-story columns assuming the other beam ends do not have vertical deformation. It is essentially a measure of axial shortening in the system and was computed for each record when the first-story drift first reaches drifts of 1% through 4% with 1% increments. Fig. 12 plots the computed MBS values as circles. Frames that collapsed at the next higher drift level are plotted in red and circumscribed with an oval.

AISC (2016c) specifies a deflection limit of 1/300 of the span for architectural serviceability requirements and 1/200 of the span for the serviceability of equipment with moveable components. Fig. 12(a) shows that the MBS levels for S4-L1-T2-C1 were well below 1/500 at 1% drift, which is commonly associated with the immediate occupancy performance level. Even at 4% drift (at the collapse prevention performance level), MBS values were mostly less than 1/200. At such a high lateral drift level, the priority is on preserving integrity over violating serviceability. When the gravity load increased in S4-L1-T3-C1, MBS was still small, and serviceability was not affected at 1% drift [Fig. 12(b)]. The MBS increased beyond 1/200 at 3% drift. However, at such a high drift level, poor structural performance is of more concern than serviceability, as also noted for S4-L1-T2-C1.

The S4-L1-T3-C1 frames with the highest MBS at 3% drift [highlighted by an oval in Fig. 12(b)] collapsed before the next drift level was reached due to global buckling of exterior columns. Comparing the MBS range at 4% drift in Fig. 12(a) (0.2–0.6% for S4-L1-T2-C1) and that at 3% drift in Fig. 12(b) (0.2–0.75% for S4-L1-T3-C1) shows that frames with similar column shortening had quite different collapse behaviors. This suggests that column shortening, in itself, does not play a direct role in collapse response. It is merely a symptom of local buckling. Excessive local buckling can be detrimental because it can reduce column end restraints, which can compromise column axial resistance and increase the potential for system collapse as the axial load demand increases.

#### **Conclusions**

The collapse behavior of steel SMFs was investigated using computational simulation. Unlike the majority of previous studies, this research used validated models capable of simulating local and global member instabilities and explicitly representing the seismic collapse response of the entire system. The models were used to study the effect of three influential parameters on system response: (1) column lateral bracing; (2) level of gravity load on the columns; and (3) column section properties. After defining clear collapse criteria, it was shown that frames can fail in either sidesway or vertical progressive collapse manners. Incremental dynamic analyses were conducted to compute the collapse fragility curves for a range of SMF designs.

The following conclusions can be drawn from the set of simulations conducted and within the limitations and assumptions outlined earlier:

- Previous component-level studies showed that web and global slenderness ratios of columns, h/tw and L/ry, have a considerable influence on the axial capacity of deep columns. The system-level studies conducted herein confirm the importance of these parameters and suggest that they not only affect member response but can also influence the collapse modes of SMFs. For example, by replacing first-story exterior columns in the TGL3 4-story frame (i.e., Pg/Py = 0.27) with a stockier section (i.e., lower h/tw and L/ry), the frame collapse capacity was significantly enhanced (median values of Sa,C and SDRmax,C increased by 34 and 76%, respectively) and the dominant collapse mode shifted to sidesway collapse from vertical collapse. Similar observations were made for the 8-story frame.
- The level of gravity load significantly influences the robustness of SMFs and their probability of collapse. For the particular 4-story frame studied in this work, axial loads of 0.2P<sub>y</sub> in first-story exterior columns appeared to be a transition point between responses dominated by sidesway and vertical collapse. Because the former is a more ductile mechanism and is preferable to the latter, it is suggested that the permissible level of gravity loads should be limited for exterior columns. Further research including a broader range of frames is necessary to select feasible values for a more general axial load limit.
- Comparing the performance of S4-L1-T3-C1 and S4-L2-T3-C1 suggests that additional lateral bracing at the level of beam bottom flanges for beam-to-column connections moderately improved the collapse capacity of SMFs (e.g., from 0.42 to 0.50 g

- for  $\tilde{S}_{a,C}$  when  $P_g/P_y=0.27$ ) and reduced the probability of vertical collapse from 11 to 8 of the 11 records. As a result, it seems prudent to recommend that beam-column connections in SMFs should be braced at both the top and bottom of the beam flanges, regardless of the column-beam moment ratios at the connection.
- Frames with similar column shortening had quite different collapse behaviors suggesting that column shortening, in itself, does not play a direct role in collapse response. It is merely a consequence of local buckling. Excessive local buckling can be detrimental because it can reduce column end restraints, which can compromise column axial resistance and increase the potential for system collapse as the axial load demand increases. Local buckling can be controlled by limiting the local slenderness ratios and axial load demand.

### Acknowledgments

This work was supported by the University of Michigan and US NSF Grant Nos. CMMI-1344372 and ACI-1638186. Any opinions, findings, conclusions, and recommendations expressed in this paper are those of the authors and do not necessarily reflect the views of the sponsor.

#### References

- AISC. 2005a. Prequalified connections for special and intermediate steel moment frames for seismic applications. ANSI/AISC 358-05. Chicago: AISC.
- AISC. 2005b. Seismic provisions for structural steel buildings. ANSI/AISC 341-05. Chicago: AISC.
- AISC. 2016a. Prequalified connections for special and intermediate steel moment frames for seismic applications. ANSI/AISC 358-16. Chicago: AISC.
- AISC. 2016b. Seismic provisions for structural steel buildings. ANSI/AISC 341-16. Chicago: AISC.
- AISC. 2016c. Specification for structural steel buildings. ANSI/AISC 360-16. Chicago: AISC.
- Arasaratnam, P., K. S. Sivakumaran, and M. J. Tait. 2011. "True stress-true strain models for structural steel elements." *ISRN Civ. Eng.* 2011: 1–11. https://doi.org/10.5402/2011/656401.
- Arias, A. 1970. "A measure of earthquake intensity." In Seismic design for nuclear power plants, edited by R. J. Hansen, 438–483. Cambridge, MA: MIT Press.
- ASCE. 2005. Minimum design loads for buildings and other structures. ASCE/SEI 7-05. Reston, VA: ASCE.
- ASCE. 2016. Minimum design loads for buildings and other structures. ASCE/SEI 7-16. Reston, VA: ASCE.
- Chi, B., and C. Uang. 2002. "Cyclic response and design recommendations of reduced beam section moment connections with deep columns." J. Struct. Eng. 128 (4): 464–473. https://doi.org/10.1061/(ASCE)0733 -9445(2002)128:4(464).
- CSA (Canadian Standard Association). 2014. *Design of steel structures*. CAN/CSA S16-09. Rexdale, ON, Canada: CSA.
- Eads, L., E. Miranda, H. Krawinkler, and D. G. Lignos. 2013. "An efficient method for estimating the collapse risk of structures in seismic regions." *Earthquake Eng. Struct. Dyn.* 42 (1): 25–41. https://doi.org/10.1002/ege.2191.
- Elkady, A., and D. G. Lignos. 2014. "Modeling of the composite action in fully restrained beam-to-column connections: Implications in the seismic design and collapse capacity of steel special moment frames." *Earthquake Eng. Struct. Dyn.* 43 (13): 1935–1954. https://doi.org/10.1002/eqe.2430.
- Elkady, A., and D. G. Lignos. 2015a. "Analytical investigation of the cyclic behavior and plastic hinge formation in deep wide-flange steel beam-columns." *Bull. Earthquake Eng.* 13 (4): 1097–1118. https://doi.org/10.1007/s10518-014-9640-y.

- Elkady, A., and D. G. Lignos. 2015b. "Effect of gravity framing on the overstrength and collapse capacity of steel frame buildings with perimeter special moment frames." *Earthquake Eng. Struct. Dyn.* 44 (8): 1289–1307. https://doi.org/10.1002/eqe.2519.
- Elkady, A., and D. G. Lignos. 2017. "Full-scale testing of deep wide-flange steel columns under multiaxis cyclic loading: Loading sequence, boundary effects, and lateral stability bracing force demands." *J. Struct. Eng.* 144 (2): 04017189. https://doi.org/10.1061/(ASCE)ST.1943 -541X.0001937.
- Engelmann, B. E., R. G. Whirley, and G. L. Goudreau. 1989. "A simple shell element formulation for large-scale elastoplastic analysis." In Analytical and computational models of shells, edited by A. K. Noor, T. Belytschko, and J. C. Simo. New York: ASME.
- FEMA. 2009. Quantification of building seismic performance factors. Rep. No. FEMA-P695. Washington, DC: FEMA.
- FEMA. 2012. Seismic performance assessment of buildings. Rep. No. FEMA-P-58. Washington, DC: FEMA.
- Fogarty, J., and S. El-Tawil. 2015. "Collapse resistance of steel columns under combined axial and lateral loading." J. Struct. Eng. 142 (1): 04015091. https://doi.org/10.1061/(ASCE)ST.1943-541X .0001350.
- Fogarty, J., T. Y. Wu, and S. El-Tawil. 2017. "Collapse response and design of deep steel columns subjected to lateral displacement." J. Struct. Eng. 143 (9): 04017130. https://doi.org/10.1061/(ASCE)ST.1943-541X .0001848.
- Hamidia, M., A. Filiatrault, and A. Aref. 2014. "Simplified seismic sidesway collapse analysis of frame buildings." *Earthquake Eng. Struct. Dyn.* 43 (3): 429–448. https://doi.org/10.1002/eqe.2353.
- Huang, Y., and S. A. Mahin. 2010. Simulating the inelastic seismic behavior of steel braced frames including the effects of low-cycle fatigue. Rep. No. PEER 2010/104. Berkeley, CA: Univ. of California at Berkeley.
- HyperMesh. 2013. HyperMesh version 12.0. Troy, MI: Altair Engineering. Ibarra, L. F., and H. Krawinkler. 2005. Global collapse of frame structures under seismic excitations. Technical Rep. 152. Stanford, CA: Stanford Univ.
- Krawinkler, H. 2009. "Loading histories for cyclic tests in support of performance assessment of structural components." In *Proc.*, 3rd Int. Conf. Advanced Experimental Structural Engineering. Berkeley, CA: Pacific Earthquake Engineering Research Center.
- LS-DYNA. 2013. LS-DYNA keyword user's manual. Livermore, CA: Livermore Software Technology.
- NIST. 2010. Evaluation of the FEMA P695 methodology for quantification of building seismic performance factors. NIST GCR 10-917-8. Gaithersburg, MD: National Institute of Standards and Technology.
- Ozkula, G., J. Harris, and C.-M. Uang. 2017. "Observations from cyclic tests on deep, wide-flange beam-columns." *Eng. J.* 54 (1): 45–59.
- Reyes-Salazar, A., M. E. Soto-Lopez, J. R. Gaxiola-Camacho, E. Bojorquez, and A. Lopez-Barraza. 2014. "Seismic response estimation of steel buildings with deep columns and PMRF." *Steel Compos. Struct.* 17 (4): 471–495. https://doi.org/10.12989/scs.2014.17.4.471.
- Shen, J.-H. J., A. Astaneh-Asl, and D. B. McCallen. 2002. Use of deep columns in special steel moment frames. Steel Tip Rep. No. 24. Moraga, CA: Structural Steel Educational Council.
- USGS. 2018. "Unified hazard tool." Accessed June 1, 2018. https://earthquake.usgs.gov/hazards/interactive/.
- Vamvatsikos, D., and C. A. Cornell. 2002. "Incremental dynamic analysis." Earthquake Eng. Struct. Dyn. 31 (3): 491–514. https://doi.org/10.1002/eqe.141.
- Wu, T.-Y., S. El-Tawil, and J. McCormick. 2017. "Behavior of steel moment frames with deep column sections under seismic loading." In *Proc.*, 16th World Conf. on Earthquake Engineering. Tokyo: International Association of Earthquake Engineering.
- Wu, T.-Y., S. El-Tawil, and J. McCormick. 2018. "Highly ductile limits for deep steel columns." *J. Struct. Eng.* 144 (4): 04018016. https://doi.org /10.1061/(ASCE)ST.1943-541X.0002002.
- Xiaoming, C., D. Jin, and L. Yungui. 2015. "Mass proportional damping in nonlinear time-history analysis." In Proc., 3rd Int. Conf. on Material, Mechanical and Manufacturing Engineering, IC3ME2015. Atlantis.

Zareian, F., H. Krawinkler, L. Ibarra, and D. Lignos. 2010. "Basic concepts and performance measures in prediction of collapse of buildings under earthquake ground motions." Struct. Design Tall Spec. Build. 19: 167–181. https://doi.org/10.1002/tal.546.

Zhang, X., and J. M. Ricles. 2006. "Experimental evaluation of reduced beam section connections to deep columns." J. Struct. Eng. 132 (3): 346–357. https://doi.org/10.1061/(ASCE)0733-9445(2006) 132:3(346).